Reconstruction of lateral root formation through single-cell RNA sequencing reveals order of tissue initiation

Laura Serrano-Ron[1,2], Pablo Perez-Garcia[1,*], Alvaro Sanchez-Corrionero[1], Inmaculada Gude[1], Javier Cabrera[1], Pui-Leng Ip[3], Kenneth D. Birnbaum[3] and Miguel A. Moreno-Risueno[1,2,*]

[1]Centro de Biotecnología y Genómica de Plantas, Universidad Politécnica de Madrid (UPM)-Instituto Nacional de Investigación y Tecnología Agraria y Alimentaria (INIA), Pozuelo de Alarcón, 28223 Madrid, Spain

[2]Departamento de Biotecnología-Biología Vegetal, Escuela Técnica Superior de Ingeniería Agronómica, Alimentaria y de Biosistemas, Universidad Politécnica de Madrid (UPM), 28040 Madrid, Spain

[3]Center for Genomics and Systems Biology, Department of Biology, New York University, New York, NY, USA

*Correspondence: Pablo Perez-Garcia (pablo.perezg@upm.es), Miguel A. Moreno-Risueno (miguelangel.moreno@upm.es)

https://doi.org/10.1016/j.molp.2021.05.028

ABSTRACT

Postembryonic organogenesis is critical for plant development. Underground, lateral roots (LRs) form the bulk of mature root systems, yet the ontogeny of the LR primordium (LRP) is not clear. In this study, we performed the single-cell RNA sequencing through the first four stages of LR formation in *Arabidopsis*. Our analysis led to a model in which a single group of precursor cells, with a cell identity different from their pericycle origins, rapidly reprograms and splits into a mixed ground tissue/stem cell niche fate and a vascular precursor fate. The ground tissue and stem cell niche fates soon separate and a subset of more specialized vascular cells form sucrose transporting phloem cells that appear to connect to the primary root. We did not detect cells resembling epidermis or root cap, suggesting that outer tissues may form later, preceding LR emergence. At this stage, some remaining initial precursor cells form the primordium flanks, while the rest create a reservoir of pluripotent cells that are able to replace the LR if damaged. Laser ablation of the central and lateral LRP regions showed that remaining cells restart the sequence of tissue initiation to form a LR. Collectively, our study reveals an ontological hierarchy for LR formation with an early and sequential split of main root tissues and stem cells.

Key words: organogenesis, patterning, stem cells, single-cell RNA-seq, cell fate, regeneration

INTRODUCTION

Postembryonic plant organogenesis requires the recruitment of specific subsets of cells known as (organ) founder cells (Chandler, 2011; Van Norman et al., 2013). Root founder cells typically give rise to lateral roots (LRs) (De Rybel et al., 2010; Motte et al., 2019; Perez-Garcia and Moreno-Risueno, 2018). The LR organogenic process initiates with asymmetric founder cell division and culminates with the formation of a new root meristem, thus generating all root cell types from a limited number of initial cells (Malamy and Benfey, 1997; Trinh et al., 2018; Motte et al., 2019).

Careful characterization of LR primordium (LRP) formation in *Arabidopsis* has led to its classification into seven developmental and/or temporal stages and the identification of central and lateral growth

domains (Malamy and Benfey, 1997), which were shown to emerge from non-deterministic cell division patterns (Lucas et al., 2013a; von Wangenheim et al., 2016). A gene regulatory network of LR formation (Lavenus et al., 2015) inferred from gravistimulated roots (Voß et al., 2015) showed dependency on AUXIN RESPONSE FACTOR (ARF) 7 for the formation of lateral growth domains of the LRP, while the central growth domain was defined by mutual inhibition between ARF7 and ARF5. PLETHORA (PLT) 3, PLT5, PLT7, and SCARECROW (SCR) factors have been shown to be expressed at the initial stages of LRP formation (Goh et al., 2016; Du and Scheres, 2017). PLT3, PLT5, and PLT7 are required for the initial formative divisions of

the LRP central domain, which leads to the specification of the LR meristem tissues; activation of PLT1, PLT2, and PLT4; and the establishment of an auxin maximum. In turn, SCR initiates the specification of the quiescent center (QC) of the new LR. These findings support a major role for genetic components in LRP patterning, indicating that cell lineages must form early during LR formation, with one of them leading to QC specification.

Organ formation has been widely studied during embryogenesis. *Arabidopsis* embryogenesis follows a highly ordered sequence of cell divisions forming stereotypic developmental stages. At the globular stage of embryogenesis the main tissue identities have been already specified, as well as the hypophysis, the precursor cell of the QC and of distal stem cells of the root (Möller et al., 2017; ten Hove et al., 2015). Thus, histogenesis in the *Arabidopsis* embryo has been understood as the simultaneous formation of multiple cell types or lineages, although more recent experiments have established the outline of a possible hierarchy during embryo tissue formation (Smit et al., 2020).

Recently, high-throughput single-cell RNA sequencing (sc-RNA-seq) of the primary root meristem has deepened our knowledge of tissue formation (Denyer et al., 2019; Jean-Baptiste et al., 2019; Ryu et al., 2019; Shulse et al., 2019; Zhang et al., 2019; Shahan et al., 2020). These studies have addressed the developmental transitions taking place to generate tissues from the stem cell niche (SCN), indicating that during primary root growth, the formation of most tissues occurs simultaneously. Tissue formation is also critical during regenerative processes. sc-RNA-seq of root regeneration upon resection of the main meristem also suggests concurrent formation of the new tissues and SCN, with early-transitioning cells showing mixed precursor identities (Efroni et al., 2016). Analysis of xylem identity through sc-RNA-seq provided a molecular mechanism for cell identity transitions and differentiation showing the importance of the underlying gene-regulatory circuit (Turco et al., 2019). Recent sc-RNA-seq profiling LR initiation during root gravistimulation has identified novel regulators of pericycle reprogramming as well as of LRP growth and stemness (Gala et al., 2021). However, powerful sc-RNA-seq approaches have not yet been applied to capture the specific cells of the early LRP, when tissue initiation presumably first occurs (Goh et al., 2016; Du and Scheres, 2017), or whether LR histogenesis follows any of the steps known from embryonic, adult, or regenerative root formation.

In this work, we have specifically isolated cells from early stages of the *Arabidopsis* LRP and performed sc-RNA-seq. We identified the initiation of six novel cell populations following three developmental branches from an initial pool of primordial cells. One of these branches involves the sequential formation of two cell populations with stem cell features and contributes to the specification of a new SCN. The second branch involves the formation of three vascular-like cell populations that might culminate in protophloem formation connecting the LRP and the primary root. The third branch initiates a cell population associated with the primordium flanks and maintaining a reservoir of primordial/pluripotent cells able to regenerate the LR if damaged. Our work shows the orderly assembly of cell lineages during LR histogenesis, suggesting the existence of hierarchical cell states of formation during post-embryonic development.

RESULTS

Transcriptional profiling of lateral root formation at the single-cell resolution

To investigate LR organogenesis, we took advantage of the ability of sc-RNA-seq to comprehensively profile cell states at given stages of development. This technique has been shown to accurately recapitulate existing cell populations and predict developmental transitions in the primary root (Denyer et al., 2019; Jean-Baptiste et al., 2019; Ryu et al., 2019; Shahan et al., 2020; Shulse et al., 2019; Zhang et al., 2019). Most LR tissues are presumably initiated from stage I to stage IV as supported by genetic evidence (Du and Scheres, 2017; Goh et al., 2016). To specifically profile early stages (I–IV) of LR formation, we used the 2 kb promoter of the *HOMEOBOX 53* (*pHB53*) transcription factor (TF) fused to the mCherry fluorescent protein and a nuclear localization signal (NLS), as this promoter specifically drives expression to early LRP cells (González-Grandío et al., 2017) (Figure 1A). LR formation occurs sequentially, following a shootward timing, and thus, LRs are at different stages of formation in the same plant. We used 4-day-old roots, which, under our growth conditions, contained a mixture of LRP from stage I to stage IV. Based on LRP quantification and number of cells in each stage of LRP development, we estimated proportions of cells of 21.8%, 20%, 24.1%, and 34.1% from stage I to IV, respectively, in our samples. Thus, our samples represented LRs at different stages of development that would need to be deconvoluted (see below). We enzymatically digested cell walls, sorted three replicates of mCherry-positive cells (using fluorescence activated cell sorting; Figure 1B) into 96-well plates, and generated cDNA libraries based on the Smart-Seq2 protocol (Picelli et al., 2014). We opted for the plate-based technique in order to provide deep per-cell read profiles of the rare but highly targeted LR cells.

Reads were processed using the R Seurat package (Butler et al., 2018; Satija et al., 2015). Quality control filters were applied to work with the more informative cells (see Methods). As a result, we selected a total of 282 highly informative cells with 362 293 mean reads/cell (Supplemental Figure 1A) and 4415 mean transcripts/cell that corresponded to 22 557 genes from the *Arabidopsis* genome. During data processing, we regressed out variability related to total number of reads, the percentage of mitochondrial genes, and the cell-cycle stage of the cells. Thus, we ensured subsequent clustering was not affected by these unwanted sources of variation (Supplemental Figure 1A–1C). Many cells were detected to have recently divided or be dividing (phases G1 and G2/M based on expression of conserved cell-cycle markers, Supplemental Table 1), as expected for an LRP in formation, which shows fast proliferation rates (Lucas et al., 2013a; von Wangenheim et al., 2016). In addition, cells collected by each replicate were distributed homogeneously, confirming reproducibility of our experimental design (Supplemental Figure 1D).

A comprehensive classification of cell populations in the LRP

Unsupervised clustering based on the transcriptomic profiles of the selected cells resulted in the identification of differentiable populations. We represented their spatial distribution by applying the
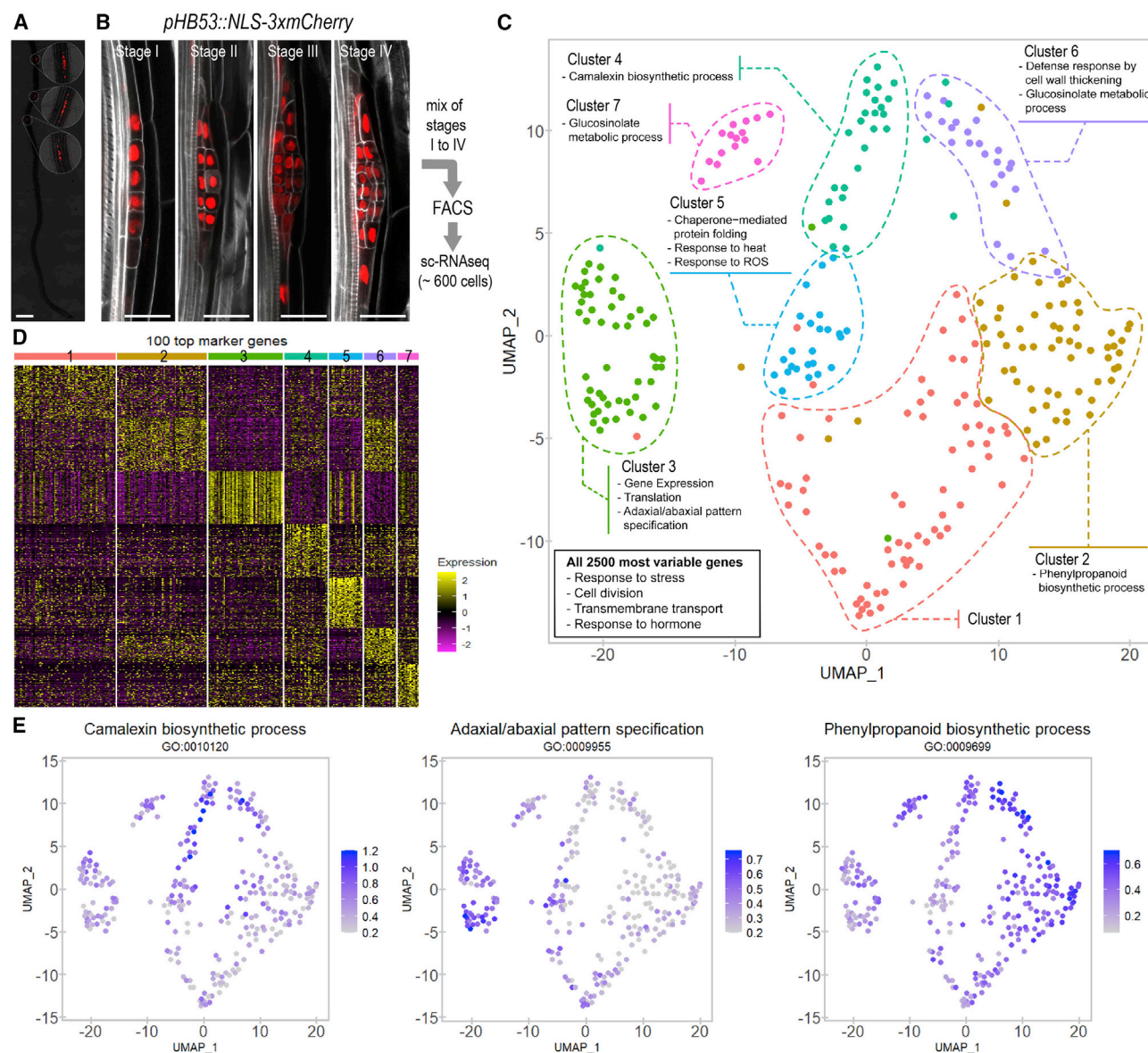
Figure 1. Distinctive cell populations can be identified through single-cell RNA sequencing (sc-RNA-seq) during early lateral root (LR) organogenesis.

(A) Overlapping fluorescent and bright-field images of a 4-day-old *Arabidopsis* seedling showing expression of the LR primordium (LRP)-specific marker *HOMEOBOX 53 mCherry* (*pHB53::NLS-3xmCherry*). Scale bar: 0.5 mm. Insets: 3.5× magnification.

(B) Confocal images showing expression of *pHB53::NLS-3xmCherry* at the LR developmental stages profiled by sc-RNA-seq. Proportion of cells in each developmental stage is indicated. Stained cell walls are shown in gray scale. Scale bars: 25 μm. FACS, fluorescence-activated cell sorting.

(C) Uniform manifold approximation and projection (UMAP) dimensional reduction of the highly informative LRP cells profiled through sc-RNA-seq. Each dot corresponds to an individual cell. Cells were clustered in seven populations and colored according to the legend. A summary of the GO terms enriched in the top 100 gene markers for each population is shown. Box: summary of enriched GO terms for the 2500 most variable genes among all populations.

(D) Heatmap showing scaled expression of the top 100 gene markers for each population in all individual cells. Cells are arranged by populations.

(E) UMAP (uniform manifold approximation and projection) plots showing the average expression of the genes annotated in three representative GO terms enriched in population 4 (left), population 3 (center), and populations 6 and 2 (right).

dimensional reduction technique uniform manifold approximation and projection (UMAP) (Becht et al., 2018). To efficiently cluster cells in Seurat based on the diversity of the dataset, a resolution parameter can be adjusted. Clustering at very low resolutions differentiated two main populations, which suggests that at least two cell identities exist at early developmental stages (Supplemental Figure 1E and 1F). Two additional clusters became distinguishable at a slightly higher resolution, suggesting a strong identity for cell populations eventually named as 3 and 5. Applying a resolution used in other root models (Ryu et al., 2019; Zhang et al., 2019) led to five different populations. Due to the highly dynamic nature of the LRP we used a less restrictive resolution (1.1) and identified six cell populations. Visual inspection allowed us to manually separate a seventh cluster

(population 7) from population 4, as it was spatially separated (Figure 1C). Comparison of the expression levels of the top 100 markers confirmed unique gene expression profiles for the seven populations identified (Figure 1D).

To investigate the functionality of these cell populations, we first analyzed the enriched gene ontology (GO) terms in the 2500 most variable genes (Supplemental Table 2) among all populations. We found terms associated with cell division, response to stress and endogenous stimuli, and transmembrane transport (Figure 1C, Supplemental Figure 2A), as expected in a rapidly forming organ where signaling might mediate pattern formation. As LRPs are known to accumulate auxin, which is required for their development (Benkova et al., 2003), we analyzed the expression of auxin polar transport genes, although auxin transport and response were not enriched GO terms. We found expression of both auxin influx- and auxin efflux-transporter genes across all the populations (Supplemental Figure 3A and 3B), which correlated well with a relatively ubiquitous auxin response in the early LRP cells (Supplemental Figure 3C and 3D). In agreement with this observation, the distribution of the auxin efflux transporters PINFORMED (PIN) 1 and PIN3, as well as the DR5 reported auxin response, did not show dramatic differences within LRP cells at very early stages of development (I and II) (Du and Scheres, 2017).

We also investigated GO enrichment in the top 100 gene markers (Supplemental Table 2) for each population and found specific GO terms, except for population 1, which did not show enrichment in any GO category (Figure 1C, Supplemental Figure 2B). Population 4 was specifically enriched in metabolism of camalexin (Figure 1C and 1E, Supplemental Figure 2B), a phytoalexin related to pathogen response and that functions as a cell-cycle regulator (Glawischnig, 2007). Population 3 showed enrichment in categories related to pattern specification, gene expression, chromatin remodeling, and epigenetics marks (Figure 1C and 1E, Supplemental Figure 2B and 2C). As cells in this population appeared to be very active transcriptionally and expressed patterning regulators, they might correspond to the central part of the LRP, since this region has been shown to contribute very actively to LRP formation (Lucas et al., 2013a). GO categories strongly represented in population 5 (Figure 1C, Supplemental Figure 3B) could be grouped into heat shock response and protein folding, categories previously associated with stem cells (de Luis Balaguer et al., 2017). The GO terms associated with populations 2 and 6 were related to callose deposition, cell-wall thickening, and phenylpropanoid metabolism, such as lignin (Figure 1C and 1E, Supplemental Figure 3B), which resembled developmental mechanisms observed in vascular tissues (Vatén et al., 2011; Xie et al., 2011; Hellmann et al., 2018).

LRP cells share the affinity to known root identities

As LR organogenesis leads to the formation of a root meristem (Trinh et al., 2018), we next explored whether the identified populations showed any quantitative affinities to root meristem cells. To systematically explore known cell identities (Supplemental Table 3), we calculated the index of cell identity scores for our single-cell dataset (Efroni et al., 2015). The majority of the cells in our dataset could not be assigned to a

known identity with a significant *p* value, which is consistent with the fact that the LRP is an organ formed *de novo*. Among the similarities found (Supplemental Figure 4), we observed that cell populations 3 and 5 presented higher scores for QC cells (~50% of relative cell identity among all the identities found), while cell populations 1, 2, 4, and 6 had the highest vasculature scores. Pericycle identity scores were very low, which agrees with LRP cells rapidly reprogramming away from their original identity. These results are consistent with early cell identity acquisition during the LR organogenesis process, with cells gaining full root tissue identities during subsequent development.

Two LRP cell populations are enriched in stem cell–like features and predict formation of the quiescent center and ground tissue lineages

As we found partial similarities to known root identities, we then used available root transcriptomes to further investigate the identity of LRP cells. As population 5 was enriched in GO categories previously associated with stem cells (de Luis Balaguer et al., 2017), we further analyzed its similarity to transcriptomes related to root stem cells. We found enrichment in gene expression associated with cortex/endodermis initials, and thus cortex/endodermis initial markers (Clark et al., 2019) were specifically expressed in population 5 (Figure 2A). A requirement for fully functional proteins or proteostasis has been associated with stem cell identity (Yan et al., 2020), and we found that chaperones with enriched expression in the endodermis or the QC (Brady et al., 2007) had enriched expression in population 5 (Figure 2B). In addition, as population 5 had affinity to QC identity (Supplemental Figure 4), it might represent a novel cell type transitioning to stem cells or to QC cells.

We next explored biomarker expression for population 5, and found the TF *C-REPEAT BINDING FACTOR 3* (*CBF3*) to be enriched in this population (Figure 2C). We used the *CBF3* promoter region to drive expression of a triple mCherry fluorescent protein fused to an NLS in a stably transformed plant line, and performed confocal laser microscopy. We first observed *pCBF3::NLS-3xmCherry* expression at stage II of LRP formation (Figure 2C); specifically, expression was observed at the central cells of the primordium on the external side. Analyses of subsequent stages of development showed that *pCBF3::NLS-3xmCherry* expression was gradually enriched in a row of cells that eventually corresponded to the endodermis/ cortex lineage or the QC of the new LR. These results suggested that population 5 must be a transitioning type of stem cell with QC and endodermis features (Figure 2D).

Continuing our search for similarities between root meristematic tissues and LRP cells, we found enriched expression of QC-related markers (Denyer et al., 2019) for population 3 and part of the endodermis/QC-transitioning stem cells (Figure 2E), including the well-known QC regulator *WUSCHEL RELATED HO-MEOBOX 5* (*WOX5*) (Sarkar et al., 2007) and the root stem cell regulator *PLT4* (Galinha et al., 2007). Additional analyses showed that expression of SCN and other QC genes (Brady et al., 2007; Zhang et al., 2019) was also enriched in population 3 and part the endodermis/QC-transitioning stem cells (Supplemental Figure 5A), suggesting that population 3 would also be related to the formation of a new QC or SCN.
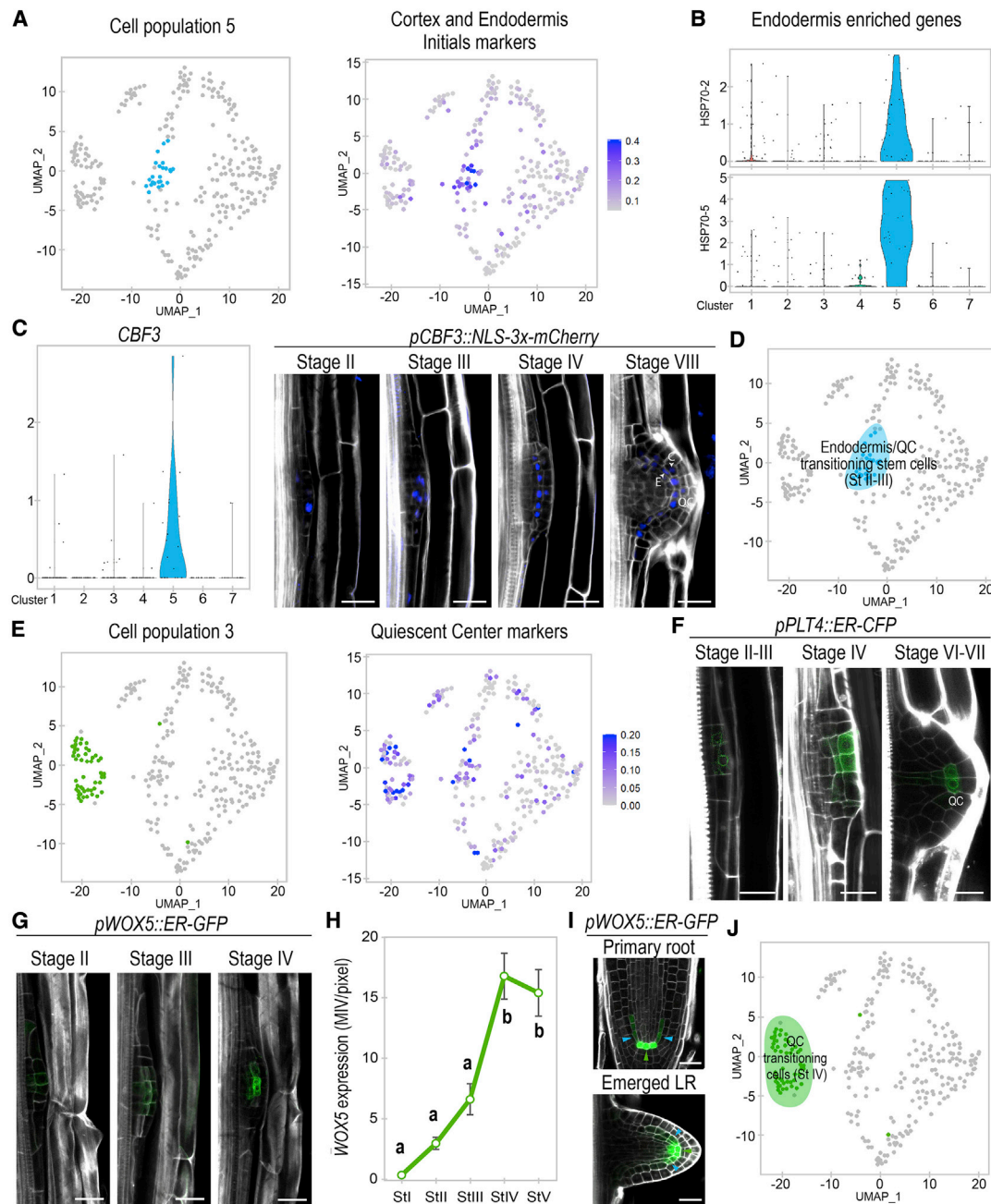
Figure 2. Two LRP cell populations are enriched in stem cell gene expression and give rise to cell lineages associated with endodermis/cortex initials and the quiescent center (QC).

(A) Left: UMAP plot showing population 5 in pale blue. Right: UMAP representation of the average expression of cortex/endodermis initial marker genes.

(B) Violin plot showing average expression of the endodermis enriched genes *HEAT SHOCK PROTEIN* (*HSP*) *70-2* and *70-5*.

(C) Left: violin plot showing expression of the population 5 biomarker *CBF3*. Right: confocal images of *pCBF3::NLS-3x-mCherry* (in blue) during LRP formation.

(D) UMAP plot defining population 5 as endodermis/QC-transitioning stem cells on a blue background.

(E) Left: UMAP plot representing population 3 in green. Right: UMAP of QC marker average expression.

(F–H) Confocal images showing **(F)** *pPLT4:CFP* and **(G)** *pWOX5::ER-GFP* expression (in green) and **(H)** quantification *pWOX5* expression from stages I to V of LR formation. MIV/pixel: mean intensity value/pixel. Different letters: $p < 0.05$ according to ANOVA and Tukey HSD *post hoc* tests. $n \geq 10$ LRPs/sample.

(I) Confocal images of *pWOX5::ER-GFP* in the primary root and an emerged LR. Green and blue arrows: cells with higher and lower expression, respectively.

(J) UMAP plot defining population 3 as QC-transitioning cells on a green background.

(C, F, G, and I) Stained cell walls are shown in gray scale. E: endodermis; C: cortex. Scale bars: 25 μm.

Next, we performed confocal laser microscopy using the markers *pWOX5::ER-GFP* and *pPLT4::ER-CFP* (Galinha et al., 2007; Sarkar et al., 2007). *pPLT4::ER-CFP* expression started at stage II/III of LRP formation. Prolonged exposure of *pPLT4::ER-CFP* showed signal in all central cells at stage II/III as previously described (Du and Scheres, 2017). However, we found that *pPLT4::ER-CFP* expression was enriched in several of the central cells on the external side (Figure 2F), which showed some overlap with *pCBF3::NLS-3xmCherry* (marking the endodermis/QC-transitioning stem cells). *pPLT4::ER-CFP* expression became stronger at stage IV and remained restricted to the central cells of the LRP (Figure 2F), while at stage V/VI it mainly coincided with the QC of the new LR. Similarly, *pWOX5::ER-GFP* expression was also low and associated with the central cells of the LRP at stages II and III (Figure 2G). Similar to *pPLT4::ER-CFP*, *pWOX5::ER-GFP* expression also greatly increased at stage IV (Figure 2H), remaining at the central area of the LRP and showing maximum expression in the cells predicted to become the new QC (Figure 2G). Inspection of the *pWOX5::ER-GFP* expression pattern in the primary root and emerged LR (Figure 2I) showed high expression levels associated with the QC, while low expression levels were associated with stem cells such as the ground tissue initials and recently formed endodermis cells. Thus, we used *pWOX5::ER-GFP* to track initiation of QC identity. A peak in *pWOX5::ER-GFP* expression occurs at stage IV of LR emergence (Figure 2H), supporting the initiation of QC identity in population 3 at stage IV. In contrast, low *pWOX5::ER-GFP* expression appears to associate with stem cells, explaining the observed overlapping between *pWOX5::ER-GFP* and the endodermis/QC-transitioning stem cell biomarker at stage II/III. These results also support that some endodermis/QC-transitioning stem cells might specialize to generate population 3 and eventually the new QC at stage IV. We define population 3 as QC-transitioning cells (Figure 2J).

Three LRP cell populations reflect early vascular-like identity acquisition

Further cell identity analysis showed that populations 1, 2, and 6 were enriched in early-stage vascular markers (Ryu et al., 2019) (Figure 3A). In addition, expression of known protophloem markers and functional regulators, such as OCTOPUS (OPS) and OBP2, as well as sieve element genes (Denyer et al., 2019; Miyashima et al., 2019; Ryu et al., 2019; Truernit et al., 2012), were enriched in population 1 (Figure 3B, Supplemental Figure 5B). The TF NAC020, which is specifically expressed in developing phloem and is upstream of the master regulator of phloem development ALTERED PHOLEM DEVELOPMENT (APL) (Kondo et al., 2016), also showed enriched expression in population 1 (Figure 3B). The largest association of cluster 1 with protophloem marker genes in comparison with clusters 2 and 6 suggested that this cell population might be more developed or differentiated. As protophloem is one of the first vascular tissues to undergo differentiation to provide meristem loading (Lucas et al., 2013b; Furuta et al., 2014), these observations suggested that several LRP cells might rapidly specialize to ensure water and nutrient supply from the primary root.

To further explore the composition of the vascular identities, we identified as biomarkers the *MYB108* and *ATHMP41* genes. *MYB108* showed enriched expression in population 2, while *ATHMP41* was specifically expressed in population 1 (Figure 3C and 3D). *ATHMP41* encodes a metal transport protein, and intriguingly, this gene and the regulator of phloem development *NAC020* showed enriched expression in a similar, coherent subset of cluster 1 (Figure 3A), suggesting that those cells might be more differentiated or constitute a cellular subtype. In agreement with this possibility, UMAP representations at very high resolutions led to the subclustering of population 1 (in subpopulations 1A, 1B, and 1C), while the rest of the populations remained largely unaltered (Supplemental Figure 6A and 6B). Notably, expression of *ATHMP41* and *NAC020* was enriched in subpopulation 1A and absent in subpopulation 1C (Supplemental Figure 6C).

We generated stable lines containing transcriptional fusions of the promoter regions of *MYB108* and *ATHMP41* to a triple yellow fluorescent protein (YFP) and an NLS. We monitored expression through confocal microscopy. We found consistent expression of *pMYB108::NLS-3xYFP* at stage III in cells adjacent to the vasculature of the primary root and located on the side of the LRP (Figure 3C). *pMYB108::NLS-3xYFP* expression decreased at stage IV, although it remained in similar locations of the LRP. Notably, *pATHMP4::NLS-3xYFP* expression started later, at stage IV (Figure 3D), while its expression pattern partially overlapped with that of *pMYB108::NLS-3xYFP*, and thus, some cells located on the side of the LRP base also showed *pATHMP4::NLS-3xYFP* expression at stage IV. The more restricted expression of *pATHMP4::NLS-3xYFP* correlates well with the predicted heterogeneity of cluster 1 and only a small portion of population 1 (or subpopulation 1A) being enriched in this biomarker expression. The cells expressing *pATHMP4::NLS-3xYFP* were adjacent to the phloem poles of the primary root, which also expressed *pATHMP4::NLS-3xYFP* (Figure 3D). At later stages of LR development *pATHMP4::NLS-3xYFP* expression remained adjacent to the phloem poles of the primary root (Figure 3E and 3F), suggesting that several cells within population 1 might specify phloem early to connect the flux of photosynthates and other potential metabolites to the LRP from the primary root.

The spatial and temporal expression patterns of *pMYB108::NLS-3xYFP* and *pATHMP4::NLS-3xYFP* support that some cells from population 2 might specialize to form population 1 and protophloem. Given that cell populations 1, 2, and 6 were arranged following a line in the UMAP representation, it appears that these cell populations could be part of a differentiation trajectory, with population 1 being more developed at one end. We designated these cell populations as vascular-like 1, vascular-like 2 and protophloem-like (Figure 3G).

Establishing the ontogeny of the early LRP

Based on our analyses, the QC-transitioning cells (stage IV) could be a specialized subset of the endodermis/QC-transitioning stem cells (stage II), while the vascular-like populations might constitute a differentiation trajectory eventually leading to phloem specification. Analysis of enrichment in root meristematic markers (Ryu et al., 2019) showed that cells located in the UMAP representation at the end of these possible developmental processes (Figure 4A; following the colored arrows) had the highest enrichment, thus being the most similar to a root
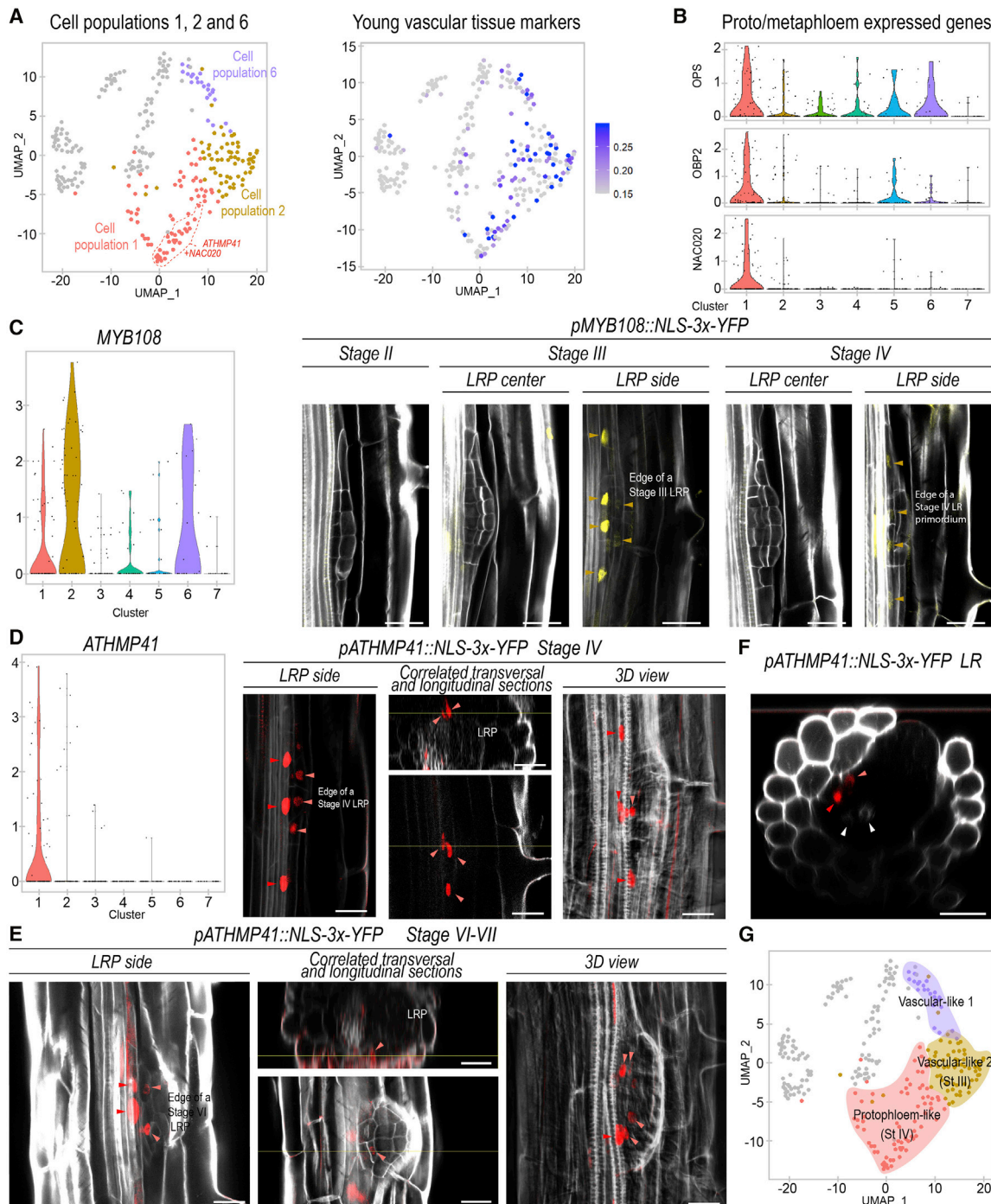
Figure 3. Different LRP cell populations show characteristic gene expression associated with vasculature development, and one of them defines the cells adjacent to the phloem tissues of primary roots.

(A) Left: UMAP plot showing cell populations 1, 2, and 6 coded by color. Cells with enriched expression of the population 1 biomarkers *ATHMP41* and *NAC020* are surrounded by a dashed red line. Right: UMAP representation of the average expression of young vascular tissue markers.

(B) Violin plot showing the average expression of protophloem and metaphloem representative genes *OCTOPUS* (*OPS*), *OBP2*, and *NAC020*.

(C) Left: violin plot showing expression of MYB108. Right: confocal images showing expression of *pMYB108:NLS-3xYFP* (in yellow) in an LRP at stages II to IV. Orange arrows: *pMYB108* marked cells.

(D) Left: violin plot showing expression of *ATHMP41*. Right: confocal images showing expression of *pATHMP41:NLS-3xYFP* (in red) at stage IV of LR formation.

(E and F) Images showing expression of *pATHMP41:NLS-3xYFP* **(E)** during LR formation and **(F)** in a recently emerged LR.

(G) UMAP plot defining populations 6, 2, and 1 as vascular-like and protophloem-like cells on colored backgrounds.

(D–F) Light red arrowheads: cells inside the LRP. Red arrowheads: primary root phloem. White arrowheads: primary root xylem. Stained cell walls are shown in gray scale. Scale bars: 25 μm.

meristem. As culmination of the LRP developmental process is a root meristem, this analysis further supports that our data can be used to infer the developmental trajectories of the LRP cells.

To investigate the ontogeny of the seven cell populations identified, we performed connectivity and pseudotime analyses. We first used partition-based graph abstraction (PAGA), which estimates the connectivity of manifold partitions (Wolf et al., 2019). We observed very strong connectivity between populations 4 and 7, and population 4 and the populations proposed to constitute a vasculature developmental trajectory (6, 2, and 1) (Figure 4B, Supplemental Figure 7A). This analysis supports that the vasculature-related populations could have originated from population 4 and form a developmental trajectory. A lower threshold showed moderate connectivity between population 4 and the endodermis/QC-transitioning stem cells among other possible connections. As a whole, the PAGA analysis suggested that population 4 might constitute a primordial cell population that would give rise to most of the LRP cells.

Next, we performed a pseudotime ordering of the cells using Monocle 3 (Cao et al., 2019). We rooted the pseudotemporal trajectory on populations 4 and vascular-like 1 based on the PAGA analysis and their lower expression of root meristematic markers. We observed a predicted trajectory from vascular-like 1 to vascular-like 2 to protophloem-like (Figure 4C), coinciding with the proposed vasculature developmental trajectory. Population 4 appeared in direct connection with the endodermis/QC-transitioning stem cells, and these cells with the QC-transitioning cells, defining a stem cell developmental trajectory, which was in agreement with some of our previous observations. Population 7 defined a third trajectory that also started from population 4. Finally, this analysis also predicted a trajectory between the endodermis/QC-transitioning stem cells and the protophloem-like population, which could relate to the fact that the former population showed certain vasculature features (Supplemental Figure 5B). Analysis of ground tissue formation during embryogenesis shows that ground tissue initials express vascular markers (Smit et al., 2020). As, based on our analysis, endodermis/QC-transitioning stem cells would give rise to the LR ground tissue, it is possible that partially overlapping ground tissue and vasculature identities could be a common feature related to ground tissue initiation.

Cell population 4 was very intriguing, as we had not found expression of any known regulators or gene markers of the primary root, and might constitute a primordial cell population giving rise to the rest of the LRP cells. As *pHB53::NLS-3xmCherry* starts to be expressed at the onset of founder cell division, this population could represent dividing founder cells or their daughters at stage I, although we did not expect to capture founder cell division consistently, given that this process occurs within ~3 h (Goh et al., 2012). Comparison of biomarkers with previous LR initiation datasets (De Smet et al., 2008; Parizot et al., 2010) showed that population 4 had the closest association (of the seven) with dividing founder cells, as expected, although only ~1/3 of the biomarkers were putative founder cell division genes (Supplemental Figure 7B). Based on this analysis, this population most likely corresponds to the founder cell daughters at stage I. We defined cell population 4 as primordial cells (Figure 4E).

Next, we constructed a transcriptional fusion of the promoter region of the identified biomarker gene *DR4* (Figure 4D), encoding a putative protease inhibitor, to drive expression of the YFP fused to an NLS and performed confocal laser microscopy. We found expression of *pDR4::NLS-3xYFP* at stage I of the LR formation (Figure 4D), in agreement with the primordial cells being a precursor state. To better understand the relationship between the primordial cells and the other LRP cells, we analyzed *pDR4::NLS-3xYFP* expression at subsequent stages of LRP development. At stage II the dividing central cells of the LRP showed weak expression of *pDR4::NLS-3xYFP* compared with the flanking cells. At later stages, we found that *pDR4::NLS-3xYFP* expression was maintained on the sides of the LRP, suggesting that cells with a slow proliferation rate might preserve the initial identity of this population. Comparison of our dataset with the LR gene-regulatory network (Lavenus et al., 2015) inferred from gravistimulated roots (Voß et al., 2015) showed that the primordial cells had the greatest dependency on ARF regulation (Supplemental Figure 7C). Notably, ARF7 regulation associates with initiation of the founder cell daughters and establishment of the LRP lateral zones. In addition, some ARF7 targets are expressed in the sides of the LRP base from stage IV to emergence (Lavenus et al., 2015), which is in agreement with the primordial cells being maintained on the sides of the LRP base. In contrast, cell fate transitions of the primordial cells were associated with fast division of the LRP central cells to give rise to the endodermis/QC-transitioning stem cells and QC-transitioning cells, which also correlated well with the QC-transitioning cells showing no dependency on ARF7 regulation (Supplemental Figure 7C).

Analysis of the characteristic features of population 7 revealed the enriched expression of *MYB36* (Supplemental Figure 5C). MYB36 is a TF expressed in the flanking regions of the LRP from stage V to emergence and defines the boundaries between proliferating and arrested cells (Fernández-Marcos et al., 2017). Given the predicted developmental trajectory from the primordial cells to cell population 7, we used *MYB36* as a biomarker gene (Figure 4F) to investigate the spatial and temporal relationships between these two cell populations. We performed confocal laser microscopy of the AraYPET recombineering construct (Liberman et al., 2015), detecting signal in several cells of the LRP flanking regions at stage IV/V. Importantly, cells in these flanking regions that showed *MYB36-AraYPET* expression also showed *DR4-YFP* expression (Figure 4D and 4F, magenta arrows), supporting the notion that population 7 could derive from a subset of the primordial cells as predicted by the developmental trajectory. We defined population 7 as flanking cells (Figure 4G).

Functional relationships among primordial cells, endodermis/QC-transitioning cells and QC-transitioning cells support a stem cell developmental trajectory

Our confocal analyses on marker expression demonstrated stage-dependent initiation for each cell population, which was spatially associated within predicted developmental trajectories (Figure 5A). Analysis of the expression of the top 100 biomarkers for each population in the LR formation dataset
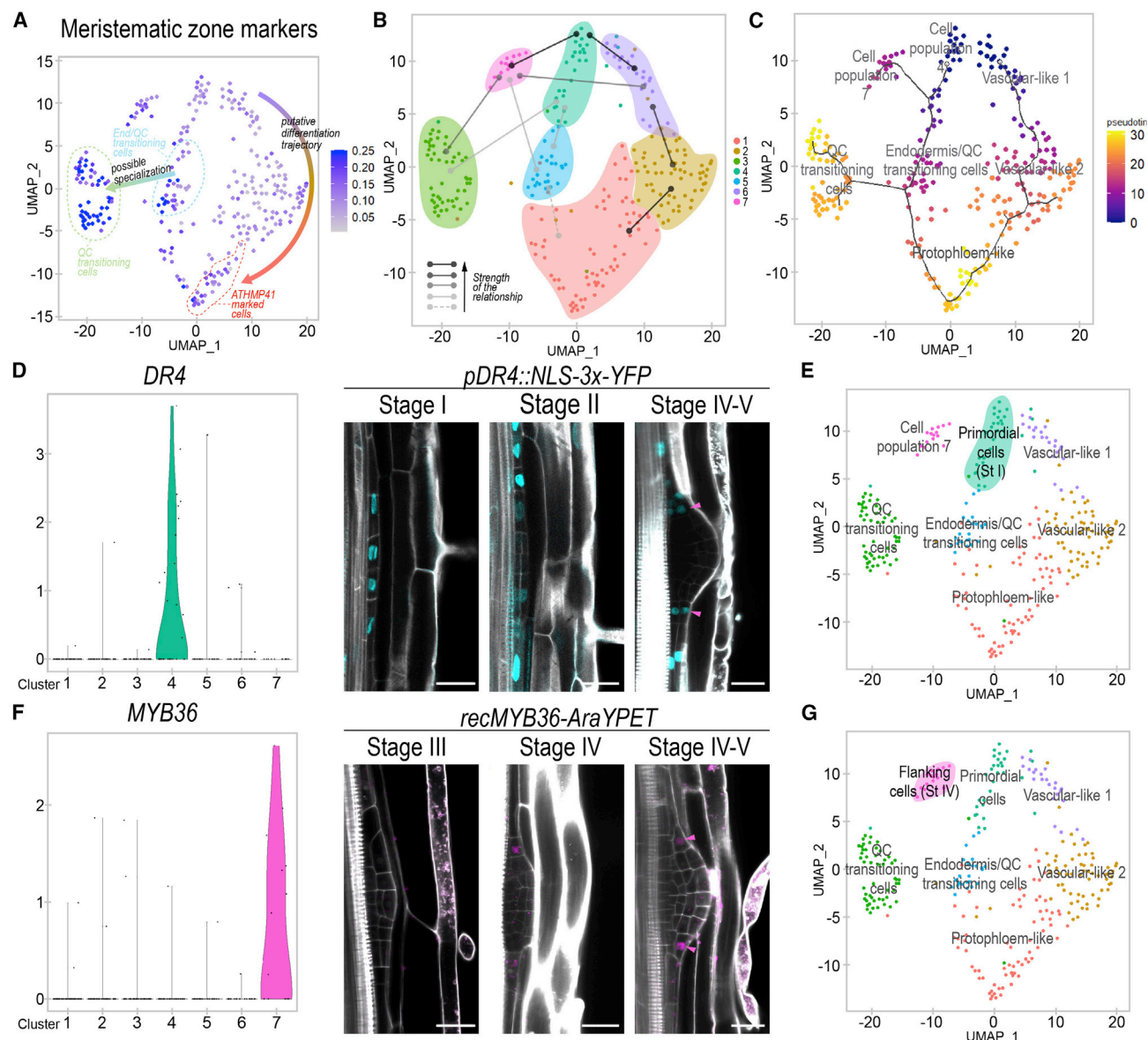
Figure 4. An early primordial cell population gives rise to three developmental trajectories during LR organogenesis.
(A) UMAP plot showing the average expression of meristematic root markers.
(B) Illustrative figure representing the results obtained from the partition-based graph abstraction analysis. Lines: relationships among populations. Strength of the relationships is displayed according to the legend.
(C) UMAP dimensional reduction plot of the pseudotemporal trajectories obtained by Monocle 3. Dark line: predicted pseudotemporal trajectories. White dots: root nodes. Dot color: pseudotime value for each cell.
(D) Left: violin plot showing expression of the population 4 biomarker *DR4*. Right: confocal images showing the expression of *pDR4:NLS-3xYFP* (in pale blue) during LRP formation.
**(E)** UMAP plot defining population 4 as primordial cells on a bluish green background.
(F) Left: violin plot showing the expression of the population 7 biomarker *MYB36*. Right: confocal images showing expression of the *MYB36-AraYPET* recombineering line (in magenta) during LRP formation.
(G) UMAP plot defining population 7 as flanking cells on a magenta background.
(D and F) Magenta arrowheads show cells in the same relative position of the LRP. Stained cell walls are shown in gray scale. Scale bars: 25 μm.

generated by gravistimulation (Voß et al., 2015) showed that early identities, such as primordial cells and vascular-like 1 cells, peaked at early time points, while late identities, such as flanking cells and QC-transitioning cells, went up later, coinciding, respectively, with stages I and IV as expected (Supplemental Figure 7D). Primordial cell biomarker expression

also went up at later times, confirming our observations that this identity is maintained on the sides during formation of the LRP base. Endodermis/QC-transitioning stem cell identity peaked at stage II, differing at later stages, while vascular-like 2 and protophloem-like identities were partially recapitulated, which could be caused by the fact that these populations share
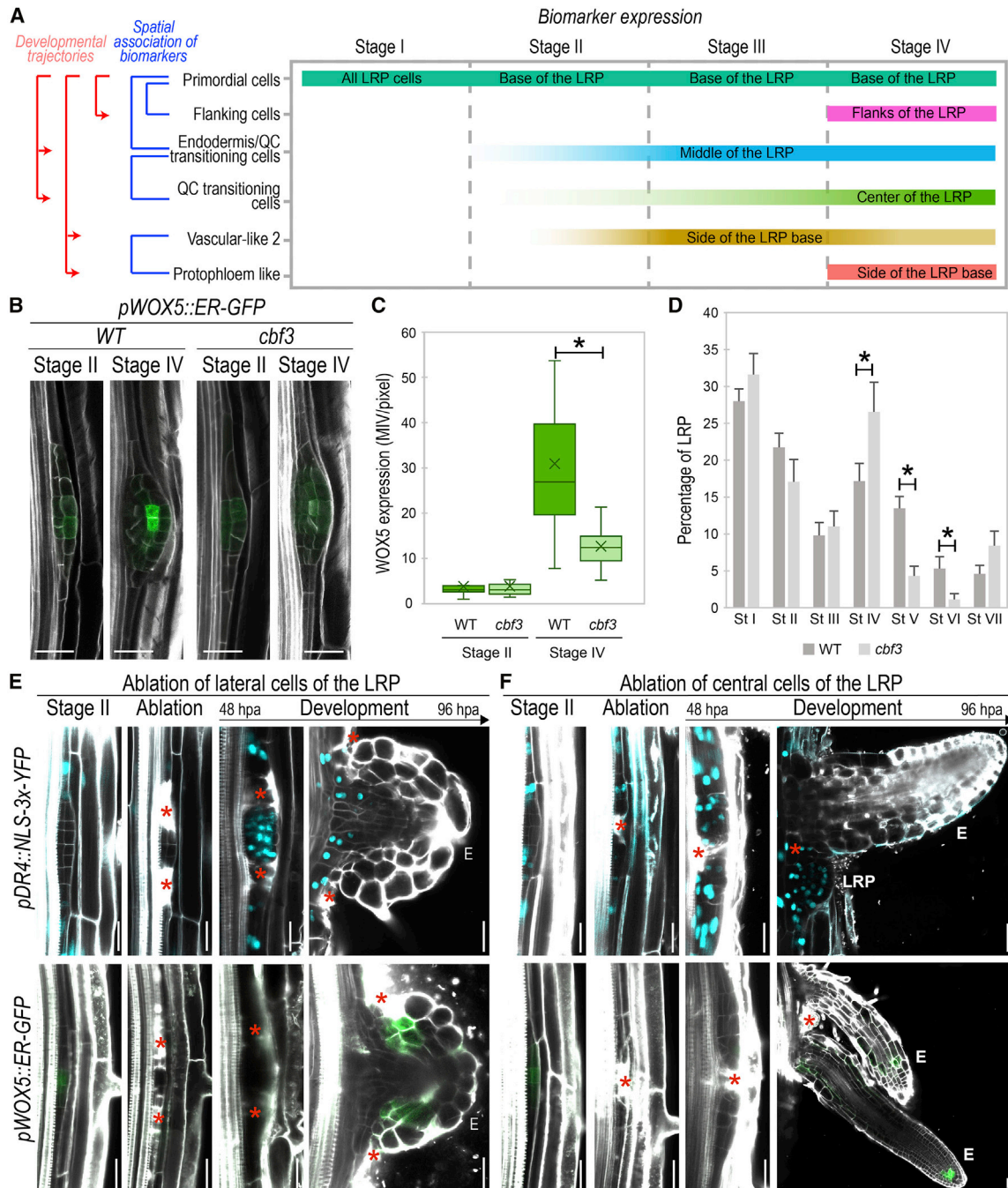
Figure 5. Functional relationships among primordial cells, endodermis/QC-transitioning cells, and QC-transitioning cells support a stem cell developmental trajectory.

(A) Schematic representation of LRP cell population initiation based on confocal microscopy analyses of biomarkers. Intensity of the color bar represents the intensity of the biomarker expression.

(B and C) (B) Confocal images showing *pWOX5::ER-GFP* expression in the wild type (WT) and in *cbf3* mutant at stages II and IV of LRP formation and **(C)** its quantification at 6 days post imbibition (dpi). Bars: boxplot whiskers. Crosses: average. MIV/pixel: mean intensity value/pixel. *$p < 0.05$ by ANOVA and Bonferroni *post hoc* test. $n \geq 15$ LRPs/sample.

(D) Quantification of LRP stages in the wild type and *cbf3* mutant at 6 dpi. *$p < 0.05$ by ANOVA and Bonferroni tests. $n \geq 25$ roots/sample.

(E and F) Confocal images showing the expression of *pDR4::NLS::3xYFP* (in cyan) and *pWOX5::ER-GFP* (in green) following laser ablation of LRP **(E)** lateral or **(F)** central cells at stage II in 5 dpi roots. hpa: hours post ablation. Red asterisks: sites of ablation. E: emerged LR; LRP: lateral root primordium.

(B, E, and F) Stained cell walls are shown in gray scale. Scale bars: 25 μm.

gene expression with the endodermis and the protophloem of the primary root, and this dataset profiles whole roots (Voß et al., 2015). All these spatial temporal associations support the initiation of new identities following a conserved sequence.

To further test LR tissue ontogeny, we focused on the stem cell developmental trajectory. Based on this trajectory, the endodermis/QC-transitioning stem cells should give rise to the QC-transitioning cells. Analysis of the mutant for the endodermis/QC-transitioning stem cell marker (*cbf3*) showed a reduction in *pWOX5::ER-GFP* expression at stage IV, whereas no change was observed at stage II compared with control roots (Figure 5B and 5C). As high *pWOX5::ER-GFP* expression at stage IV was associated with specification of the QC-transitioning cells, the observed reduction in *pWOX5::ER-GFP* expression in *cbf3* indicates altered specification of this cell population. When we analyzed LRP formation in *cbf3*, we observed abnormal accumulation of LRP at stage IV, while LRP in the subsequent developmental stages V and VI decreased, confirming that initiation of QC-transitioning cells from endodermis/QC-transitioning stem cells is required for LRP development.

Next, we performed laser ablation of the LRP central and lateral regions at stage II in plants carrying the primordial cell population marker (*pDR4::NLS-3x-YFP*) and *pWOX5::ER-GFP*. Ablation of the LRP lateral regions resulted in inactivation of *pWOX5::ER-GFP* and activation of *pDR4::NLS-3x-YFP* expression in the remaining cells to resume LRP formation and, eventually, to express *pWOX5::ER-GFP* again (Figure 5E). Thus, ablation of the lateral regions of the LRP appeared to restart the sequence of identity initiation predicted by the stem cell developmental trajectory to form a new LR. Ablation of the LRP central region caused fast division of the primordial cells in the laterals to form two adjacent LRPs or LRs, which indicates that all primordial cells have similar formative capacities regardless of their position or origins. In agreement with the proposed stem cell developmental trajectory, cells marked with *pDR4::NLS-3x-YFP* did not show *pWOX5::ER-GFP* expression (Figure 5F) (i.e., if they correspond to the large daughter cells or are immediately derived from them).

Taken together, these results show the functional relevance of the endodermis/QC-transitioning stem cells, a previously unknown cell population, and the existence of a stem cell developmental trajectory that initiates cell identities following a conserved interconnected sequence.

The primordial cells constitute a pluripotent cell reservoir and associate with camalexin metabolite

As ablation of the central side of the LRP resulted in division of the remaining primordial cells to form new LRs, we wondered if the primordial cells might maintain their identity and functionality after LR emergence. We observed *pDR4::NLS-3x-YFP* expression at the base of emerged LR (Figure 6A). Furthermore, expression of the founder cell marker *pSKP2Bs::NLS-3x-mCherry* (Perianez-Rodriguez et al., 2021) was also found at the base of emerged LRs, suggesting that primordial cells remained and might be functional. Next, we excised LRs and observed that new LRs emerged from the root regions containing the *pDR4::NLS-3x-YFP* and *pSKP2Bs::NLS-3x-mCherry* marked

cells (Figure 6B), indicating that primordial cells appear to form new LRs when the initial LR was damaged.

The camalexin biosynthesis pathway was a GO term enriched in the primordial cells (Figure 1C and 1E), so we decided to further explore this association. When plants were treated with acivicin, which has been shown to inhibit camalexin biosynthesis in *Arabidopsis* (Su et al., 2011), we found activation of *pDR4::NLS-3x-YFP* expression in the central cells of the LRP at stage II, while *pCBF3::NLS-3x-mCherry* expression was turned off (Figure 6C and 6D). Supplementation of roots with both acivicin and camalexin restored *pDR4::NLS-3x-YFP* expression to the LRP sides and *pCBF3::NLS-3x-mCherry* expression to the central region of the LRP. When we analyzed LRP formation in roots treated with acivicin, we observed that LRP did not develop normally, accumulating at stage II. However, this developmental inhibition could be partially reversed when the roots were additionally supplemented with camalexin (Figure 6E), which suggests that initiation of endodermis/QC-transitioning stem cells at stage II is critical for LRP development. Finally, as activating *pDR4::NLS-3x-YFP* expression is accompanied by turning off of *pCBF3::NLS-3x-mCherry* and vice versa (Figure 6C and 6D), it can be inferred that primordial and endodermis/QC-transitioning stem cell identities are part of a conserved sequence, further supporting the stem cell developmental trajectory and the associated role of camalexin.

DISCUSSION

Our research has identified seven cell populations formed during the early stages of LR organogenesis. Five of them constitute completely novel cell types, while the QC-transitioning cells represent a precursor state of the LR QC, and the primordial cells likely correspond to the stage I founder cell daughters. Interestingly, our results show the same identity for all these cells, although they are formed by a division morphologically asymmetric. We have also determined the spatial localization of six of these cell populations within the LRP and their temporal order of formation, which is hierarchical and conserved. We also established functional relationships among several of them that validate one of the three inferred developmental trajectories. Our research reveals the ontogeny of LRP tissue initiation with an unprecedented level of resolution. Furthermore, we demonstrate the functionality of the primordial cells at the sides of the LRP base to regenerate new LRs following laser ablation and LR resection. We also identified novel transcriptomic features of the primordial cells that led to the identification of camalexin as a new LRP developmental regulator associated with initiation of endodermis/QC-transitioning stem cells.

The ontogeny of LRP is organized and involves the hierarchical assembly of cell lineages

Based on the spatial localization of the cell populations, the order of formation and the developmental branch to which they belong (i.e., the capacity of the cell populations to give rise or derive from other cell populations), we propose a model for LRP patterning during organogenesis (Figure 7A). In this model the spatial organization of the populations in layers would be determined by the position of the precursor population. Thus, the vascular-like 1 cells (on the inside) and the endodermis/QC-transitioning
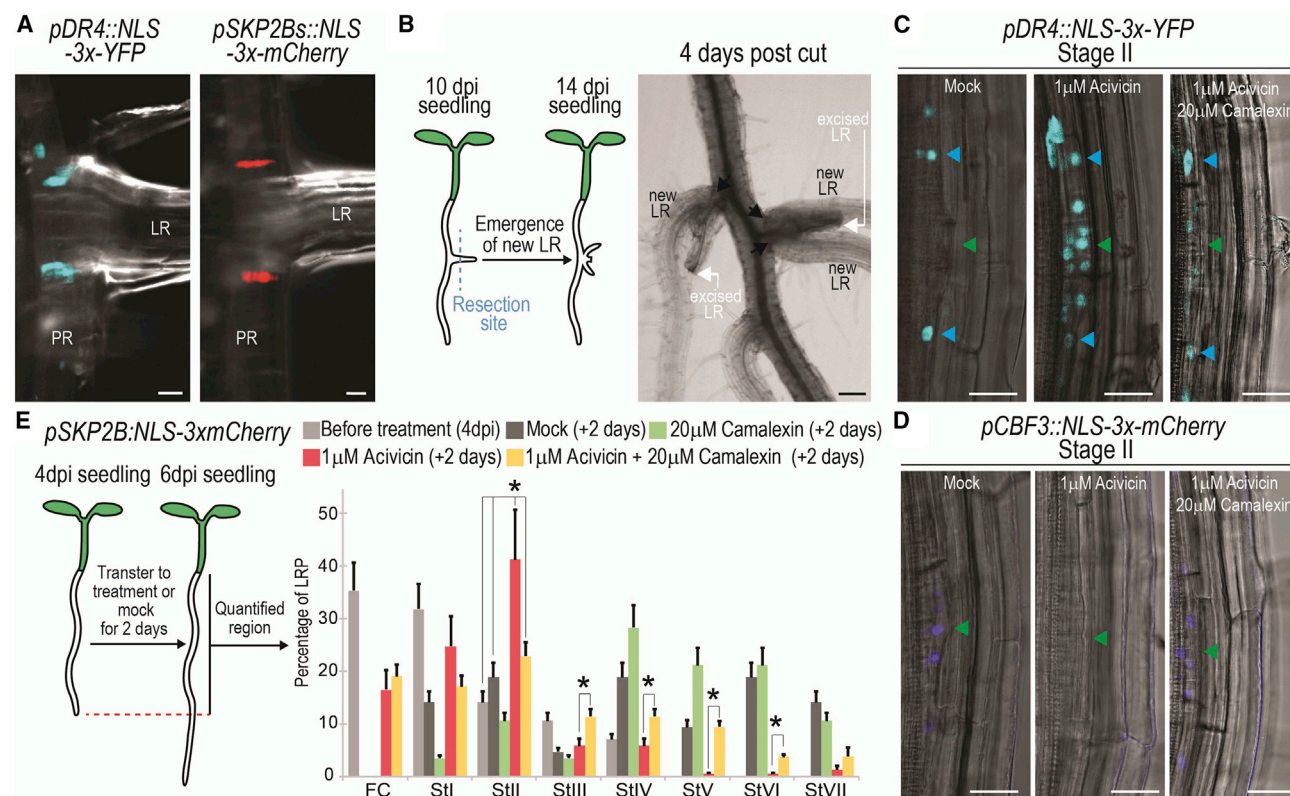
Figure 6. The primordial cells constitute a reservoir for pluripotent cells and associate with camalexin metabolite.

(A) Confocal images showing expression of the marker for the primordial cells, *pDR4:NLS-3xYFP*, and the founder cell marker, *pSKP2Bs:NLS-3xmCherry*, at the base of emerged LRs.

(B) Left: cartoon illustrating experiment. Right: bright-field image showing formation of new LRs after excision of emerged LRs. Black arrowheads: sites of emergence.

(C and D) Confocal images showing expression of **(C)** *pDR4:NLS-3xYFP* and **(D)** *pCBF3:NLS-3xmCherry* in 4 dpi roots treated with 1 μM acivicin or with 1 μM acivicin and 20 μM camalexin for 2 days. Acivicin is a camalexin biosynthesis inhibitor. Green and cyan arrows: central and lateral LRP regions, respectively.

(E) Acivicin and camalexin regulate LRP formation. Left: cartoon illustrating experiment. Right: quantification of LRP stages following treatments. *$p < 0.05$ by ANOVA and Bonferroni tests. $n \geq 20$ roots/condition. Scale bars: 25 μm **(A, C, and D)** and 125 μm **(B)**.

stem cells (on the outside) would be derived at stage II/III from the primordial cells. Undivided or slow-dividing cells on the sides would remain as primordial cells, whereas several of them would specialize at stage IV into the flanking cells to eventually establish the growth boundaries of the LRP. Some of the endodermis/QC-transitioning stem cells in the central region would form the QC-transitioning cells at stage IV to subsequently generate a QC and maybe other SCN cells. The remaining endodermis/QC-transitioning stem cells would establish the ground tissue lineage.

Based on this model, the LRP regulator SCR (Goh et al., 2016) would be expressed in the endodermis/QC-transitioning stem cells (a novel cell type), likely contributing to initiation of the QC-transitioning cells to specify a new QC. In agreement with the proposed additional pathways leading to QC specification (Goh et al., 2016), we found CBF3 to specifically regulate initiation of the QC-transitioning cells. In addition, the PLT factors (Du and Scheres, 2017) could also belong to the same stem cell developmental trajectory. PLT3/5/7 could regulate initiation of the endodermis/QC-transitioning stem cells and PLT1/2/4 initiation of the QC-

transitioning cells, which could require additional positional signals such as auxin. Future experiments might investigate the role of ARF7 in primordial cell fate specification and its maintenance after LR emergence.

In the vascular development branch (Figure 7A), vascular-like 1 would initiate vascular-like 2 cells at stage III, while at stage IV, some of these would have transitioned to protophloem-like cells. Intriguingly, the cells putatively becoming protophloem would be the cells adjacent to the phloem tissues of the primary root, which anticipates vasculature connection and suggests that signals from primary root tissues might induce their specialization. In agreement with this idea, during grafting, genes related to vascular tissue formation are activated above and below the graft junction, which is part of a recognition mechanism that leads to reconnection of vasculature tissues (Melnyk et al., 2018). Interestingly, grafting does not involve establishment of stem cells, and neither does the vasculature developmental trajectory in the LRP show stem cell features.

Our analyses did not identify any cell population with affinity to epidermis or lateral-root-cap cells, suggesting that these tissues
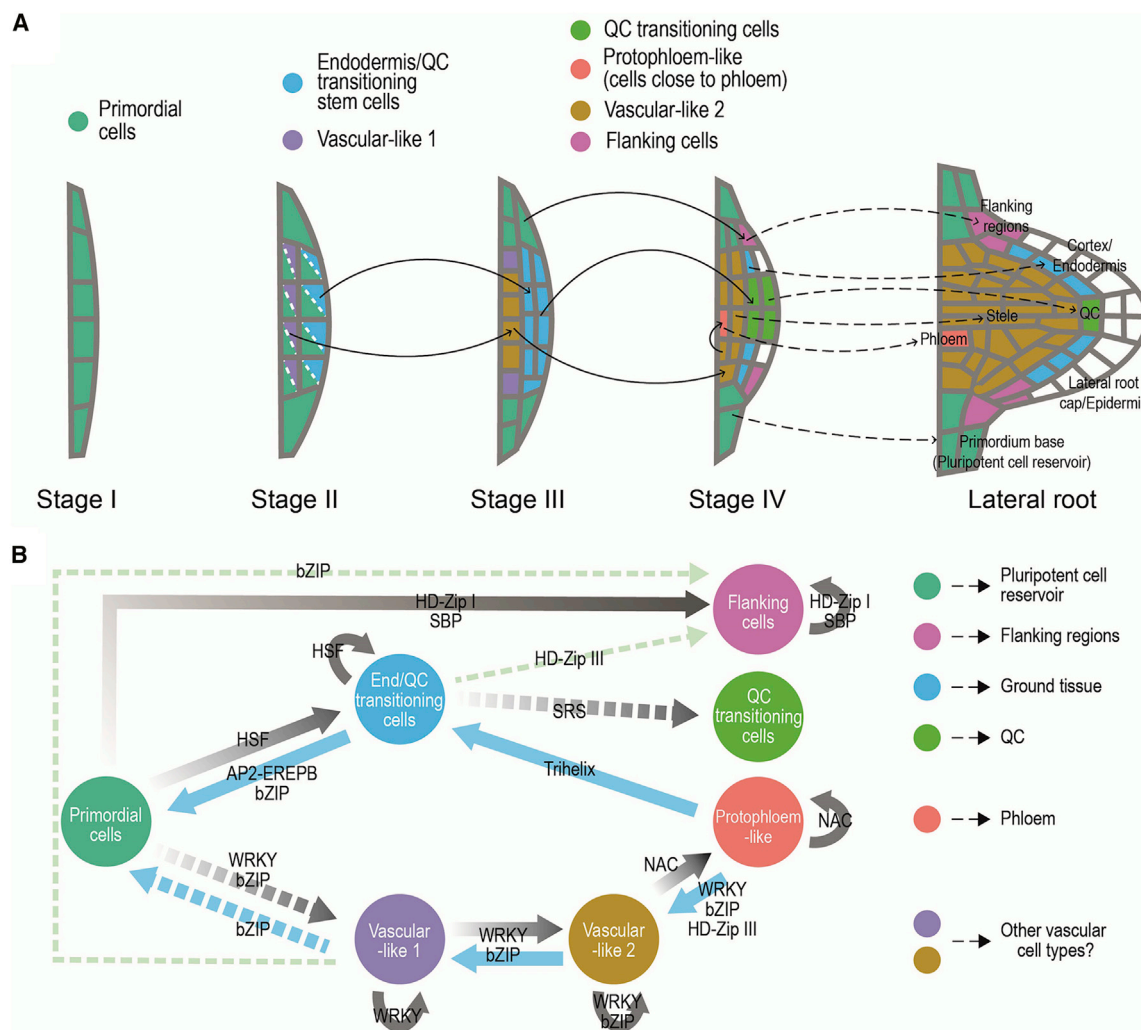
Figure 7. The proposed model for LRP patterning during organogenesis.
(A) The localization of the different cell populations is represented by colors as indicated. The model is based on the capacity of the populations to give rise to or derive from other cell populations (black arrows) based on their spatial localization, sequential order of formation, and developmental branch. The dashed arrows indicate subsequent tissues or regions of the LR would originate from each cell population based on the localization of biomarkers at stage IV or later if evaluated. In our model, LR external layers (epidermis and lateral root cap) would be formed after stage IV of LR formation.
(B) Hypothetical regulation among the different LRP cell populations based on PAGA and pseudotime analyses (Figure 4B and 4C) and enrichment in TF families and TF binding sites (TFBS) (Supplemental Table 4). Continuous lines: relationships predicted by PAGA, Monocle, and TF/TFBS enrichment analyses. Discontinuous lines: relationships predicted by the TF/TFBS enrichment analysis and either PAGA or Monocle. Gray lines: regulation through a developmental trajectory. Note that all the TF families putatively mediating transitions also self-regulate the newly formed population (except SRS). Blue lines: additional regulation within a developmental trajectory. Pale green lines: regulation between different developmental trajectories.

might be formed at later developmental stages, possibly from QC-transitioning cells according to their localization or other undetermined cells. Further supporting this idea, expression of the columella and epidermis regulators FEZ and WEREWOLF, respectively, was observed at developmental stages close to LR emergence (Du and Scheres, 2017).

Regulation of the developmental trajectories of LRP

In addition to the identification of CBF3 as a regulator of LRP ontogeny, our research also has the potential of identifying novel molecular interactions. As a proof of concept, we analyzed enrichment of TF families and TF binding sites (TFBS) in the seven cell populations of the early LRP. We found at least one specific family of TFs to be enriched in a population and its corresponding TFBSs to be enriched in the temporally subsequent (or precursor) population (Figure 7B, Supplemental Table 4). Thus, one can infer the putative role of class I homeodomain–leucine zipper (HD-ZIP) TFs mediating the transition from primordial to flanking cells, which could lead to *MYB36* activation, or that of HD-ZIP III TFs and SHI RELATED SEQUENCE (SRS) proteins mediating the transition from endodermis/QC-transitioning stem cells to QC-transitioning cells, among others. Interestingly, SRS proteins regulate auxin biosynthetic genes, favoring the local induction of auxin maxima (Eklund et al., 2010), which would be in agreement with an expected auxin maximum present at the future domain of the LR QC.

In some other cases, the same family of TFs was enriched along an entire developmental trajectory, such as the WRKY TFs (Figure 7B). WRKY18 was specifically expressed in the primordial cells, while subsequent vascular-like 1/2 were enriched in WRKY binding sites and in other WRKY TFs. WRKY18 has been shown to form a complex with histone acetyltransferases to activate sugar-response genes (Chen et al., 2019), and in addition sugar response has been associated with vascular reconnection (Melnyk et al., 2018), suggesting that sugar or nutrient response might be involved in the specialization of the vasculature trajectory. In addition, NAC TFs such as NAC020 might mediate the transition from vascular-like 2 to protophloem-like cells. NAC020 is specifically expressed in protophloem-like cells and is upstream of the regulator of phloem development APL (Kondo et al., 2016). Moreover, we observed enrichment of the vasculature regulators PHLOEM EARLY DOF TFs (PEAR) (Miyashima et al., 2019) in the protophloem-like cells. PEAR genes have been shown to activate expression of HD-ZIP III TFs, and we found HD-ZIP III TFs to be enriched in the same cells. As HD-ZIP III TFs are negative regulators of vasculature proliferation (Miyashima et al., 2019), their activation might facilitate the specification of protophloem-like cells.

Organ formation in plants involves the specification of new cell identities and their organization in tissues or growth domains. Previous research in tissue ontogeny showed limited hierarchy or no obvious order of formation. Our findings provide an insight into a possible tissue formation mechanism that involves the hierarchical assembly or initiation of tissues, thus shedding light on the long-term question of how plants conduct developmental programs to establish cell fate while growing or developing structures.

METHODS

Plant material and growth conditions

Arabidopsis thaliana Columbia-0 (Col-0) accession was the genetic background used in this study. Seeds were surface-sterilized upon exposure to Cl_2 gas and stratified in sterile water at 4°C in darkness for 2 days. After stratification, the seeds were transferred to Petri dishes containing half-Murashige & Skoog medium with 1% sucrose and 10 g/L plant agar (Duchefa). Acivicin (Thermo Fisher, Waltham, MA, USA) and camalexin (Avantor, Radnor, PA, USA) were added to the growth medium at the indicated concentrations. *Arabidopsis* seedlings were vertically grown in chambers under a 16/8 photoperiod at 22°C. *pWOX5::ER-GFP* (Sarkar et al., 2007), *pPLT4:: ER-CFP* (Du and Scheres, 2017), *RecMYB36::AraYPET* (Liberman et al., 2015), and *pSKP2Bs::NLS-3x-mCherry* (Perianez-Rodriguez et al., 2021) lines were also used in this study.

Protoplast isolation and sc-RNA-seq

Biological samples were extracted from plants expressing the *pHB53:NLS-3xmCherry* construct at 4 days of growth (i.e., post imbibition) after stratification. These roots showed 49%, 22%, 17%, and 12% LRP from stages I to IV, which we estimated corresponded to 21.8%, 20%, 24.1%, and 34.1% of cells in each stage, respectively. For each independent replicate, the primary root tip and the aerial part of ~400 plants were removed and the remaining roots were subjected to 1.5 h of protoplasting as detailed in Efroni et al. (2016). The cell suspension containing mCherry-positive cells was sorted on a FACSAria II (Becton Dickinson) into 96-well plates using the single-cell sort mode. Three replicates were processed on a Bravo robotic system (Agilent) and a Mantis (Formulatrix) using the cDNA construction and bar-coding protocol

detailed in Efroni et al. (2016) to construct cDNA libraries. Libraries were generated based on the Smart-Seq2 protocol (Picelli et al., 2014) using the Nextseq 500 mid output 150 v.2.5 kit and run on the Illumina Nextseq 500. This approach yielded 573 single cells, which represent over five-fold coverage of all the cells contained in the LRP from stage I to IV. Reads were trimmed using Trimmomatics with the following settings: Illumina clip, 2:30:10; crop, 48; sliding window, 4:5; minleng, 36. Then they were mapped to the *Arabidopsis* genome reference using Star, with default settings, using the –quantMode GeneCounts argument to generate counts in Star (Efroni et al., 2016). The data were deposited in GEO under accession no. GSE161970.

Generation of a single-cell gene expression matrix

Raw count processing and subsequent analysis were performed in R (https://www.R-project.org/) using Seurat (v.3.1) (Satija et al., 2015; Butler et al., 2018) unless indicated. Cutoff parameters for the 573 sequenced cells required at least 1000 total reads, between 200 and 8000 transcripts, and between 0.1% and 6% of mitochondrial genes per cell. In addition, we removed transcripts expressed in fewer than three cells. The expression data were log normalized to generate an expression matrix reflecting the expression of 22 557 transcripts across 282 cells, with 362 293 mean reads/cell and 4415 mean transcripts/cell. Cell-cycle stage was estimated for each cell based on expression of G2/M and S phase markers (Supplemental Table 1) using the Seurat function CellCycleScoring(), which assigns a score. For subsequent clustering the expression matrix data were modeled using the Seurat function ScaleData() to regress out the variability for the total number of reads, percentage of mitochondrial genes, and cell-cycle stage. To regress out the cell-cycle stage of the cells, the relationship between gene expression and the S and G2M cell-cycle scores was calculated. The scaled residuals of remaining genes were used for subsequent dimensional reduction, avoiding clustering cells based on their cell-cycle stage, reads, or mitochondrial genes. Using the expression matrix, genes differentially expressed among clusters ($p < 0.01$, log-fold-change ≥ 0.25, present in $\geq$25% cells) were identified as biomarkers. Protoplasting-induced genes (Birnbaum, 2003) were excluded from transcriptomic analyses.

Data analysis and clustering

Dimensionality reduction by principal-component analysis was performed using the top 2500 most variable features in Seurat (v.3.1) (Supplemental Table 2). The top five principal components were determined as informative using the Elbow plot and Jack Straw plot in Seurat and used as input for clustering and visualization using UMAP (Becht et al., 2018). Clusters were identified using Seurat at different resolutions as indicated. Heatmaps were performed in Seurat.

Assessment of cell identity and gene expression analysis

The index of cell identity was calculated in R according to gene expression in the Root Map (Brady et al., 2007; Efroni et al., 2016). Spec values were also calculated in R using the following parameters: cuts = 4 and distshape = 1. Biomarkers for known cell types were selected according to previous studies (Brady et al., 2007; Efroni et al., 2016; Clark et al., 2019; Denyer et al., 2019; Ryu et al., 2019) as specified in Supplemental Table 3. Specific identity features in our dataset were performed by analyzing the average expression of known cell-type biomarkers: QC markers from Brady et al. (2007) and Denyer et al. (2019), SCN markers (cluster 12 enriched genes) from Zhang et al. (2019), cortex/ endodermis initial markers from Clark et al. (2019), young vascular markers from Ryu et al. (2019), and protophloem markers from Denyer et al. (2019) and Ryu et al. (2019). Meristematic markers were those in Huang and Schiefelbein (2015).

GO enrichment analysis

GO enrichment analyses were performed in g:Profiler (Raudvere et al., 2019) using $p < 0.001$ to detect the GO terms enriched in the 2500 most

variable genes and the top 100 markers for each cluster. Visualization of GO enrichment in UMAP plots was performed using the average expression of all the genes included in those GO terms according to the TAIR database.

Pseudotime analyses

Pseudotemporal relationships among single cells were assessed by two different methods: PAGA (Wolf et al., 2019) and Monocle 3 (Cao et al., 2019). Clustering from Seurat was used as the initial input, so identities were not reestablished by these methods.

TF and TF binding site enrichment

TF and TFBS enrichment was performed using the Agris and AthaMap databases, respectively (Davuluri et al., 2003; Steffens, 2004). As input for TF and TFBS search, we used the top 100 markers for each population and the 500 bp upstream and 50 bp downstream of each gene. Enrichment was calculated as the ratio between the TFs found in each population and those in the set of the 2500 most variable genes or those provided by AthaMap. Enriched TFs or TFBSs were those with a ratio ≥1.5 (Supplemental Table 4).

Selection, cloning, and transformation of marker genes

The 2 kb promoter of *HB53* (AT5G66700) was amplified by PCR (Phusion High-Fidelity DNA polymerase, Thermo Fisher Scientific) using the primers 5′-GTTCGTTGCCCACACATTACT-3′ and 5′-TTTCTCTCTCTAGTTTTT-CAGAC-3′. The identification of markers upregulated in each cluster compared with the rest of the cells was performed in Seurat (v.3.1). The promoter regions of selected marker genes were amplified by PCR (Phusion High-Fidelity DNA polymerase, Thermo Fisher Scientific) using the primers 5′-CTCCTTGACTTACAGACCAAAC-3′ and 5′- GGTGGCCTTC ATGATTGTTTC-3′ for *DR4* (AT1G73330), 5′-ACTTCTTTGCTTCACATAAG TTAAAAGTCA-3′and 5′-TGATCAGAAGAGTACTCTGTTTCAAGA-3′ for *CBF3* (AT4G25480), and 5′-GTGCCCTGGAATCTAACATT-3′ and 5′-CTT GTTGATTTTATCTTTGACTT-3′ for *ATHMP41* (AT4G39700). Construct cloning was performed using the MultiSite Gateway Three-Fragment Vector Construction Kit (Invitrogen) to fuse promoter regions to an NLS and three repeats of the YFP or mCherry fluorescent protein genes in the dpGreen BarT vector as indicated. Constructs were transformed into the Col-0 background by the floral dip method. Homozygous lines were selected among the T2 progeny in ammonium glufosinate (Merck).

Microscopy and regeneration assays

Four- to six-day-old seedlings from homozygous lines were stained with 10 mg/ml propidium iodide (Sigma-Aldrich) or 1 mg/ml SCRI Renaissance 2200 dye (SR2200) (Renaissance Chemicals) and imaged in a Leica SP8 laser-scanning confocal microscope (Leica) using a hybrid detector counting mode and the following settings: YFP or AraYPET (excitation 514 nm, acquisition 524–544 nm), mCherry (excitation 561 nm, acquisition 600–650 nm), SR2200 (excitation 405 nm, acquisition 430–450 nm), and propidium iodide (excitation 561 nm, acquisition 600–630 nm). Quantification of fluorescent signal was performed in Leica LAS AF Lite software as pixel density. Laser ablation of cells was performed using pulses of lasers of 405 nm and 458 nm for 1 min. Fluorescence microscopy was performed in a Flumazone (Leica M205FA adapted with a Hamamatsu EMCCD X2 camera). LR resection was performed using a scalpel in Flumazone.

Statistical analysis

Statistical differences were detected using R. Homoscedastic groups were analyzed using ANOVA and Tukey HSD or Bonferroni *post hoc* tests for one or more factors, respectively. Significant differences were collected with 5% level of significance.

SUPPLEMENTAL INFORMATION

Supplemental Information is available at *Molecular Plant Online*.

REFERENCES

Becht, E., McInnes, L., Healy, J., Dutertre, C.-A., Kwok, I.W.H., Ng, L.G., Ginhoux, F., and Newell, E.W. (2018). Dimensionality reduction for visualizing single-cell data using UMAP. Nat. Biotechnol. **37**:38–44.

Benkova, E., Michniewicz, M., Sauer, M., Teichmann, T., Seifertova, D., Jurgens, G., and Friml, J. (2003). Local, efflux-dependent auxin gradients as a common module for plant organ formation. Cell **115**:591–602.

Birnbaum, K. (2003). A gene expression map of the Arabidopsis root. Science **302**:1956–1960.

Brady, S.M., Orlando, D.A., Lee, J.Y., Wang, J.Y., Koch, J., Dinneny, J.R., Mace, D., Ohler, U., and Benfey, P.N. (2007). A high-resolution root spatiotemporal map reveals dominant expression patterns. Science **318**:801–806.

Butler, A., Hoffman, P., Smibert, P., Papalexi, E., and Satija, R. (2018). Integrating single-cell transcriptomic data across different conditions, technologies, and species. Nat. Biotechnol. **36**:411–420.

Cao, J., Spielmann, M., Qiu, X., Huang, X., Ibrahim, D.M., Hill, A.J., Zhang, F., Mundlos, S., Christiansen, L., Steemers, F.J., et al. (2019). The single-cell transcriptional landscape of mammalian organogenesis. Nature **566**:496–502.

Chandler, J.W. (2011). Founder cell specification. Trends Plant Sci **16**:607–613. https://doi.org/10.1016/j.tplants.2011.08.005.

Chen, Q., Xu, X., Xu, D., Zhang, H., Zhang, C., and Li, G. (2019). WRKY18 and WRKY53 coordinate with HISTONE ACETYLTRANSFERASE1 to regulate rapid responses to sugar. Plant Physiol. **180**:2212–2226.

Clark, N.M., Buckner, E., Fisher, A.P., Nelson, E.C., Nguyen, T.T., Simmons, A.R., de Luis Balaguer, M.A., Butler-Smith, T., Sheldon, P.J., Bergmann, D.C., et al. (2019). Stem-cell-ubiquitous

genes spatiotemporally coordinate division through regulation of stem-cell-specific gene networks. Nat. Commun. **10**:5574.

Davuluri, R.V., Sun, H., Palaniswamy, S.K., Matthews, N., Molina, C., Kurtz, M., and Grotewold, E. (2003). AGRIS: Arabidopsis Gene Regulatory Information Server, an information resource of Arabidopsis cis-regulatory elements and transcription factors. BMC Bioinformatics **4**:25.

de Luis Balaguer, M.A., Fisher, A.P., Clark, N.M., Fernandez-Espinosa, M.G., Möller, B.K., Weijers, D., Lohmann, J.U., Williams, C., Lorenzo, O., and Sozzani, R. (2017). Predicting gene regulatory networks by combining spatial and temporal gene expression data in Arabidopsis root stem cells. Proc. Natl. Acad. Sci. U S A **114**:E7632–E7640.

De Rybel, B., Vassileva, V., Parizot, B., Demeulenaere, M., Grunewald, W., Audenaert, D., Van Campenhout, J., Overvoorde, P., Jansen, L., Vanneste, S., et al. (2010). A novel aux/IAA28 signaling cascade activates GATA23-dependent specification of lateral root founder cell identity. Curr. Biol. **20**:1697–1706.

De Smet, I., Vassileva, V., De Rybel, B., Levesque, M.P., Grunewald, W., Van Damme, D., Van Noorden, G., Naudts, M., Van Isterdael, G., De Clercq, R., et al. (2008). Receptor-like kinase ACR4 restricts formative cell divisions in the Arabidopsis root. Science **322**:594–597.

Denyer, T., Ma, X., Klesen, S., Scacchi, E., Nieselt, K., and Timmermans, M.C.P. (2019). Spatiotemporal developmental trajectories in the Arabidopsis root revealed using high-throughput single-cell RNA sequencing. Dev. Cell **48**:840–852.e5.

Du, Y., and Scheres, B. (2017). PLETHORA transcription factors orchestrate de novo organ patterning during Arabidopsis lateral root outgrowth. Proc. Natl. Acad. Sci. U S A **114**:11709–11714.

Efroni, I., Ip, P.-L., Nawy, T., Mello, A., and Birnbaum, K.D. (2015). Quantification of cell identity from single-cell gene expression profiles. Genome Biol. **16**:9.

Efroni, I., Mello, A., Nawy, T., Ip, P.-L., Rahni, R., DelRose, N., Powers, A., Satija, R., and Birnbaum, K.D. (2016). Root regeneration triggers an embryo-like sequence guided by hormonal interactions. Cell **165**:1721–1733.

Eklund, D.M., Ståldal, V., Valsecchi, I., Cierlik, I., Eriksson, C., Hiratsu, K., Ohme-Takagi, M., Sundström, J.F., Thelander, M., Ezcurra, I., et al. (2010). The Arabidopsis thaliana STYLISH1 protein acts as a transcriptional activator regulating auxin biosynthesis. Plant Cell **22**:349–363.

Fernández-Marcos, M., Desvoyes, B., Manzano, C., Liberman, L.M., Benfey, P.N., del Pozo, J.C., and Gutierrez, C. (2017). Control of Arabidopsis lateral root primordium boundaries by MYB36. New Phytol. **213**:105–112.

Furuta, K.M., Yadav, S.R., Lehesranta, S., Belevich, I., Miyashima, S., Heo, J.o., Vaten, A., Lindgren, O., De Rybel, B., Van Isterdael, G., et al. (2014). Arabidopsis NAC45/86 direct sieve element morphogenesis culminating in enucleation. Science **345**:933–937.

Gala, H.P., Lanctot, A., Jean-Baptiste, K., Guiziou, S., Chu, J.C., Zemke, J.E., George, W., Queitsch, C., Cuperus, J.T., and Nemhauser, J.L. (2021). A single cell view of the transcriptome during lateral root initiation in Arabidopsis thaliana. Plant Cell, koab101. https://doi.org/10.1101/2020.10.02.324327.

Galinha, C., Hofhuis, H., Luijten, M., Willemsen, V., Blilou, I., Heidstra, R., and Scheres, B. (2007). PLETHORA proteins as dose-dependent master regulators of Arabidopsis root development. Nature **449**:1053–1057.

Glawischnig, E. (2007). Camalexin. Phytochemistry **68**:401–406.

Goh, T., Joi, S., Mimura, T., and Fukaki, H. (2012). The establishment of asymmetry in Arabidopsis lateral root founder cells is regulated by

LBD16/ASL18 and related LBD/ASL proteins. Development **139**:883–893.

Goh, T., Toyokura, K., Wells, D.M., Swarup, K., Yamamoto, M., Mimura, T., Weijers, D., Fukaki, H., Laplaze, L., Bennett, M.J., et al. (2016). Quiescent center initiation in the Arabidopsis lateral root primordia is dependent on the SCARECROW transcription factor. Development **143**:3363–3371.

González-Grandío, E., Pajoro, A., Franco-Zorrilla, J.M., Tarancón, C., Immink, R.G.H., and Cubas, P. (2017). Abscisic acid signaling is controlled by a BRANCHED1/HD-ZIP I cascade in Arabidopsis axillary buds. Proc. Natl. Acad. Sci. U S A **114**:E245–E254.

Hellmann, E., Ko, D., Ruonala, R., and Helariutta, Y. (2018). Plant vascular tissues—connecting tissue comes in all shapes. Plants **7**:109.

Huang, L., and Schiefelbein, J. (2015). Conserved gene expression programs in developing roots from diverse plants. Plant Cell **27**:2119–2132.

Jean-Baptiste, K., McFaline-Figueroa, J.L., Alexandre, C.M., Dorrity, M.W., Saunders, L., Bubb, K.L., Trapnell, C., Fields, S., Queitsch, C., and Cuperus, J.T. (2019). Dynamics of gene expression in single root cells of Arabidopsis thaliana. Plant Cell **31**:993–1011.

Kondo, Y., Nurani, A.M., Saito, C., Ichihashi, Y., Saito, M., Yamazaki, K., Mitsuda, N., Ohme-Takagi, M., and Fukuda, H. (2016). Vascular cell induction culture system using Arabidopsis leaves (VISUAL) reveals the sequential differentiation of sieve element-like cells. Plant Cell **28**:1250–1262.

Lavenus, J., Goh, T., Guyomarc'h, S., Hill, K., Lucas, M., Voss, U., Kenobi, K., Wilson, M.H., Farcot, E., Hagen, G., et al. (2015). Inference of the Arabidopsis lateral root gene regulatory network suggests a bifurcation mechanism that defines primordia flanking and central zones. Plant Cell **27**:1368–1388.

Liberman, L.M., Sparks, E.E., Moreno-Risueno, M.A., Petricka, J.J., and Benfey, P.N. (2015). MYB36 regulates the transition from proliferation to differentiation in the Arabidopsis root. Proc. Natl. Acad. Sci. U S A **112**:12099–12104.

Lucas, M., Kenobi, K., von Wangenheim, D., Vobeta, U., Swarup, K., De Smet, I., Van Damme, D., Lawrence, T., Peret, B., Moscardi, E., et al. (2013a). Lateral root morphogenesis is dependent on the mechanical properties of the overlaying tissues. Proc. Natl. Acad. Sci. U S A **110**:5229–5234.

Lucas, W.J., Groover, A., Lichtenberger, R., Furuta, K., Yadav, S.-R., Helariutta, Y., He, X.-Q., Fukuda, H., Kang, J., Brady, S.M., et al. (2013b). The plant vascular system: Evolution, development and FunctionsF. J. Integr. Plant Biol. **55**:294–388.

Malamy, J.E., and Benfey, P.N. (1997). Organization and cell differentiation in lateral roots of Arabidopsis thaliana. Development **124**:33–44.

Melnyk, C.W., Gabel, A., Hardcastle, T.J., Robinson, S., Miyashima, S., Grosse, I., and Meyerowitz, E.M. (2018). Transcriptome dynamics at Arabidopsis graft junctions reveal an intertissue recognition mechanism that activates vascular regeneration. Proc. Natl. Acad. Sci. U S A **115**:E2447–E2456.

Miyashima, S., Roszak, P., Sevilem, I., Toyokura, K., Blob, B., Heo, J.-o., Mellor, N., Help-Rinta-Rahko, H., Otero, S., Smet, W., et al. (2019). Mobile PEAR transcription factors integrate positional cues to prime cambial growth. Nature **565**:490–494.

Möller, B.K., ten Hove, C.A., Xiang, D., Williams, N., López, L.G., Yoshida, S., Smit, M., Datla, R., and Weijers, D. (2017). Auxin response cell-autonomously controls ground tissue initiation in the earlyArabidopsisembryo. Proc. Natl. Acad. Sci. U S A **114**:E2533–E2539.

Motte, H., Vanneste, S., and Beeckman, T. (2019). Molecular and environmental regulation of root development. Annu. Rev. Plant Biol. **70**:465–488.

Parizot, B., De Rybel, B., and Beeckman, T. (2010). VisuaLRTC: a new view on lateral root initiation by combining specific transcriptome data sets. Plant Physiol. **153**:34–40.

Perez-Garcia, P., and Moreno-Risueno, M.A. (2018). Stem cells and plant regeneration. Dev. Biol. **442**:3–12.

Perianez-Rodriguez, J., Rodriguez, M., Marconi, M., Bustillo-Avendaño, E., Wachsman, G., Sanchez-Corrionero, A., De Gernier, H., Cabrera, J., Perez-Garcia, P., Gude, I., et al. (2021). An auxin-regulable oscillatory circuit drives the root clock in Arabidopsis. Sci. Adv. **7**:eabd4722.

Picelli, S., Faridani, O.R., Björklund, Å.K., Winberg, G., Sagasser, S., and Sandberg, R. (2014). Full-length RNA-seq from single cells using Smart-seq2. Nat. Protoc. **9**:171–181.

Raudvere, U., Kolberg, L., Kuzmin, I., Arak, T., Adler, P., Peterson, H., and Vilo, J. (2019). g:Profiler: a web server for functional enrichment analysis and conversions of gene lists (2019 update). Nucleic Acids Res. **47**:W191–W198.

Ryu, K.H., Huang, L., Kang, H.M., and Schiefelbein, J. (2019). Single-cell RNA sequencing resolves molecular relationships among individual plant cells. Plant Physiol. **179**:1444–1456.

Sarkar, A.K., Luijten, M., Miyashima, S., Lenhard, M., Hashimoto, T., Nakajima, K., Scheres, B., Heidstra, R., and Laux, T. (2007). Conserved factors regulate signalling in Arabidopsis thaliana shoot and root stem cell organizers. Nature **446**:811–814.

Satija, R., Farrell, J.A., Gennert, D., Schier, A.F., and Regev, A. (2015). Spatial reconstruction of single-cell gene expression data. Nat. Biotechnol. **33**:495–502.

Shahan, R., Hsu, C.-W., Nolan, T.M., Cole, B.J., Taylor, I.W., Vlot, A.H.C., Benfey, P.N., and Ohler, U. (2020). A single cell Arabidopsis root atlas reveals developmental trajectories in wild type and cell identity mutants. bioRxiv https://doi.org/10.1101/2020.06.29.178863.

Shulse, C.N., Cole, B.J., Ciobanu, D., Lin, J., Yoshinaga, Y., Gouran, M., Turco, G.M., Zhu, Y., O'Malley, R.C., Brady, S.M., et al. (2019). High-throughput single-cell transcriptome profiling of plant cell types. Cell Rep. **27**:2241–2247.e4.

Smit, M.E., Llavata-Peris, C.I., Roosjen, M., van Beijnum, H., Novikova, D., Levitsky, V., Sevilem, I., Roszak, P., Slane, D., Jürgens, G., et al. (2020). Specification and regulation of vascular tissue identity in the Arabidopsis embryo. Development **147**:dev186130.

Steffens, N.O. (2004). AthaMap: an online resource for in silico transcription factor binding sites in the Arabidopsis thaliana genome. Nucleic Acids Res. **32**:368D–372D.

Su, T., Xu, J., Li, Y., Lei, L., Zhao, L., Yang, H., Feng, J., Liu, G., and Ren, D. (2011). Glutathione-Indole-3-Acetonitrile is required for camalexin biosynthesis in Arabidopsis thaliana. Plant Cell **23**:364–380.

ten Hove, C.A., Lu, K.J., and Weijers, D. (2015). Building a plant: cell fate specification in the early Arabidopsis embryo. Development **142**:420–430.

Trinh, C.D., Laplaze, L., and Guyomarc'h, S. (2018). Lateral Root Formation: Building a Meristem de novo (Hoboken, NJ: Wiley), pp. 847–890.

Truernit, E., Bauby, H., Belcram, K., Barthelemy, J., and Palauqui, J.C. (2012). OCTOPUS, a polarly localised membrane-associated protein, regulates phloem differentiation entry in Arabidopsis thaliana. Development **139**:1306–1315.

Turco, G.M., Rodriguez-Medina, J., Siebert, S., Han, D., Valderrama-Gómez, M.Á., Vahldick, H., Shulse, C.N., Cole, B.J., Juliano, C.E., Dickel, D.E., et al. (2019). Molecular mechanisms driving switch behavior in xylem cell differentiation. Cell Rep. **28**:342–351.e4.

Van Norman, J.M., Xuan, W., Beeckman, T., and Benfey, P.N. (2013). To branch or not to branch: the role of pre-patterning in lateral root formation. Development **140**:4301–4310. https://doi.org/10.1242/dev.090548.

Vatén, A., Dettmer, J., Wu, S., Stierhof, Y.-D., Miyashima, S., Yadav, S.R., Roberts, C.J., Campilho, A., Bulone, V., Lichtenberger, R., et al. (2011). Callose biosynthesis regulates symplastic trafficking during root development. Dev. Cell **21**:1144–1155.

von Wangenheim, D., Fangerau, J., Schmitz, A., Smith, R.S., Leitte, H., Stelzer, E.H., and Maizel, A. (2016). Rules and self-organizing properties of post-embryonic plant organ cell division patterns. Curr. Biol. **26**:439–449.

Voß, U., Wilson, M.H., Kenobi, K., Gould, P.D., Robertson, F.C., Peer, W.A., Lucas, M., Swarup, K., Casimiro, I., Holman, T.J., et al. (2015). The circadian clock rephases during lateral root organ initiation in Arabidopsis thaliana. Nat. Commun. **6**:7641.

Wolf, F.A., Hamey, F.K., Plass, M., Solana, J., Dahlin, J.S., Göttgens, B., Rajewsky, N., Simon, L., and Theis, F.J. (2019). PAGA: graph abstraction reconciles clustering with trajectory inference through a topology preserving map of single cells. Genome Biol. **20**:59.

Xie, B., Wang, X., Zhu, M., Zhang, Z., and Hong, Z. (2011). CalS7 encodes a callose synthase responsible for callose deposition in the phloem. Plant J. **65**:1–14.

Yan, P., Ren, J., Zhang, W., Qu, J., and Liu, G.-H. (2020). Protein quality control of cell stemness. Cell Regen. **9**:22.

Zhang, T.-Q., Xu, Z.-G., Shang, G.-D., and Wang, J.-W. (2019). A single-cell RNA sequencing profiles the developmental landscape of Arabidopsis root. Mol. Plant **12**:648–660.